JPET Fast Forward. Published on June 13, 2019 as DOI: 10.1124/jpet.119.257543
This article has not been copyedited and formatted. The final version may differ from this version.

Modeling Corticosteroid Pharmacokinetics & Pharmacodynamics – III: Estrous Cycle- and Estrogen Receptor-Dependent Antagonism of GILZ Enhancement by Corticosteroids

Vivaswath S. Ayyar, Debra C. DuBois, Richard R. Almon, William J. Jusko

Department of Pharmaceutical Sciences, State University of New York at Buffalo, Buffalo, NY (V.S.A., D.C.D., R.R.A., W.J.J.) and Department of Biological Sciences, State University of New York at Buffalo, Buffalo, NY (D.C.D., R.R.A.)

Running Title: Systems Modeling of Corticosteroid-Estrogen Antagonism

Corresponding author:

William J. Jusko, Ph.D.

Department of Pharmaceutical Sciences

School of Pharmacy and Pharmaceutical Sciences

State University of New York at Buffalo

Buffalo, NY, 14214

E-mail: wjjusko@buffalo.edu

Telephone: 716-645-2855

Fax: 716-829-6569

Number of text pages: 25

Number of tables: 4

Number of figures: 7

Number of references: 45

Number of words:

Abstract: 247

Significance Statement: 105

Introduction: 743

Discussion: 1595 (limit exceeded to address reviewer's comment)

List of non-standard abbreviations: 17β-estradiol, E_2; ADX, adrenalectomized; AUEC, area under the effect curve; CS, corticosteroid; CST, corticosterone; E, estrus; ER, estrogen receptor; GILZ, glucocorticoid-induced leucine zipper; GR, glucocorticoid receptor; GRE, glucocorticoid response element; HPA, hypothalamic-pituitary-adrenal; MPL, methylprednisolone; PE, proestrus; mPBPK, minimal physiologically based pharmacokinetic; PD, pharmacodynamic; PG, pharmacogenomic

Recommended Section: Drug Metabolism, Transport, and Pharmacogenomics

ABSTRACT

Our previous report examined the pharmacokinetics (PK) of methylprednisolone (MPL) and adrenal suppression following a 50 mg/kg intramuscular bolus in male and female rats. The development of a minimal physiologically-based pharmacokinetic/pharmacodynamic (mPBPK/PD) model was described. In continuation of such assessments, we investigated sex differences in genomic MPL responses (PD). Message expression of the glucocorticoid-induced leucine zipper (GILZ) was chosen as a multi-tissue biomarker of glucocorticoid receptor (GR)-mediated drug response. Potential time-dependent interplay between sex hormone and glucocorticoid signaling *in vivo* was assessed by comparing the enhancement of GILZ by MPL in uterus [high estrogen receptor (ER) density] and in liver (lower ER density) from males and females dosed within the proestrus (high estradiol/progesterone) and estrus (low estradiol/progesterone) phases of the rodent estrous cycle. An expanded systems PD model of MPL considering circadian rhythms, multi-receptor (ER and GR) control, and estrous variations delineated the determinants controlling receptor/gene-mediated steroid responses. Hepatic GILZ response was ~3-fold higher in females, regardless of estrous stage, compared to males, driven predominantly by increased MPL exposure in females and a negligible influence of estrogen interaction. In contrast, GILZ response in uterus during proestrus in females was 60% of that observed in estrus-phased females, despite no PK or receptor differences, providing *in vivo* support to the hypothesis of estrogen-mediated antagonism of glucocorticoid signaling. The developed model offers a mechanistic platform to assess the determinants of sex- and tissue-specificity in corticosteroid actions and, in turn, reveals a unique PD drug-hormone interaction occurring *in vivo*.

JPET Fast Forward. Published on June 13, 2019 as DOI: 10.1124/jpet.119.257543
This article has not been copyedited and formatted. The final version may differ from this version.

Significance

Mechanisms relating to sex-based pharmacodynamic variability in genomic responses to corticosteroids have been unclear. Using combined experimental and systems pharmacology modeling approaches, sex differences in both pharmacokinetic and pharmacodynamic mechanisms controlling the enhancement of a sensitive corticosteroid-regulated biomarker, the glucocorticoid-induced leucine zipper (GILZ), were clarified *in vivo*. The multiscale minimal PBPK/PD model successfully captured the experimental observations and quantitatively discerned the roles of the rodent estrous cycle (hormonal variation) and tissue specificity in mediating the antagonistic co-regulation of GILZ gene synthesis. These findings collectively support the hypothesis that estrogens antagonize pharmacodynamic signaling of genomic corticosteroid actions *in vivo* in a time- and estrogen receptor-dependent manner.

Introduction

The corticosteroids (CS) exert diverse biochemical effects in numerous tissues. Most adverse and therapeutic actions of CS occur in tissues upon drug binding the glucocorticoid receptors (GR). The CS can cause effects which are rapid in onset, such as cell trafficking and adrenal suppression (Yao et al., 2008). In contrast, pharmacogenomic (PG) regulation by the drug-receptor complex occurs in a delayed manner (Jusko, 1995) due to a series of intracellular transduction steps, including gene regulation and consequent mRNA and protein synthesis. Several generations of increasingly mechanistic pharmacokinetic and pharmacodynamic (PK/PD) models of gene-mediated steroid actions have been developed (Nichols et al., 1989; Xu et al., 1995; Sun et al., 1998; Ramakrishnan et al., 2002; Mager et al., 2003; Hazra et al., 2007b; Ayyar et al., 2018). These models have demonstrated that the major determinants of steroid response include: i) disposition characteristics of the steroid, ii) relative receptor affinity of the steroid, iii) availability of cytosolic receptors, and iv) system control of the biomarker(s) (mRNA and protein) that mediate end-point responses.

Our early studies employed the adrenalectomized (ADX) male rat model to examine CS actions. The use of ADX animals obviated complicating factors such as the influence of endogenous glucocorticoids. This experimental paradigm was subsequently evolved to examine the PK/PD effects of MPL in intact (non-ADX) male rats, with consideration of endogenous steroid effects and circadian rhythms (Hazra et al., 2007b). These assessments were, however, confined to males. Sex is a relevant factor influencing the PK/PD of drugs. Despite this recognition, very few preclinical PK/PD studies to date include sex as a variable. The overarching goal of this work was to expand our mechanistic assessments of MPL PK/PD from intact male rats to females with consideration of estrous cycle variations.

Our companion report (Ayyar et al., 2019a) compared the plasma and tissue PK of MPL as well as the time-course of corticosterone (CST) suppression by MPL following a 50 mg/kg IM bolus in male and female rats. Prominent sex differences were observed in PK, with higher drug exposures in females,

regardless of estrous stage. No sex difference in plasma protein binding of MPL was observed (Ayyar et al., 2019b). Robust suppression of plasma CST occurred in both sexes upon dosing. Sex- and estrous-dependent differences in basal CST rhythms (Atkinson and Waddell, 1997) were considered.

Sex differences in the receptor/gene-mediated mechanisms of MPL have not been investigated thus far. The glucocorticoid-induced leucine zipper (GILZ) is a sensitive CS-regulated gene which has emerged as an important mediator of anti-inflammatory CS actions (Ayroldi and Riccardi, 2009). The characterization of GILZ as a multi-tissue biomarker for CS PK/PD/PG effects has been reported in male rats (Ayyar et al., 2015; Ayyar et al., 2017). Mechanistic experiments in a human uterine epithelial cell line indicated that enhancement of GILZ mRNA and protein by dexamethasone (DEX) was potently antagonized in the presence of 1 - 10 pM of estradiol (Whirledge and Cidlowski, 2013; Whirledge et al., 2013). The siRNA-mediated knock-down of the estrogen receptor (ER) reversed the antagonism, suggestive of an ER-dependent mechanism. Chromatin immunoprecipitation analysis revealed that GR and ER recruitment to a specific GRE site in the GILZ promoter region was decreased in the presence of both DEX and estradiol compared to their respective ligand alone (Whirledge and Cidlowski, 2013), indicative of a competitive antagonistic interaction occurring at the molecular level.

GILZ expression was chosen as a biomarker in our studies to investigate sex-, tissue-, and estrous cycle-dependent variability in the receptor/gene-mediated PD activity of MPL. The time-course of GILZ enhancement after MPL dosing was quantified in liver – a tissue with high GR and relatively low ER; and in uterus – a tissue with lower GR and a high ER content (Izawa et al., 1984; Kuiper et al., 1997; Plowchalk and Teeguarden, 2002). Organs were harvested from male rats and also from females dosed within two distinct phases of their reproductive cycle; when systemic concentrations of estradiol were either low (estrus; E) or elevated (proestrus; PE) (Smith et al., 1975). It was hypothesized that elevated estradiol production during PE in females would antagonize MPL-enhanced GILZ mRNA expression in tissues with ER. This final report of a three-part series focused on i) characterizing potential sex- and tissue-dependent differences in GILZ mRNA dynamics following MPL, and ii) developing a minimal physiologically-based pharmacokinetic/PD/PG (mPBPK/PD/PG) systems model of MPL considering

circadian rhythms, multi-receptor control, and the rodent estrous cycle to delineate in a quantitative manner the multi-factorial control of genomic steroid responses *in vivo*.

Materials and Methods

Animal study designs, care of animals, and procedures for collection of tissue samples are described in Part II.

Plasma Estradiol Determination

The plasma concentrations of estradiol in normal (non-dosed) E- and PE-phased female rats were quantified using a competitive enzyme-linked immunosorbent assay (ELISA) kit (LifeSpan BioSciences, Seattle, WA). Rat plasma samples were used undiluted. All other procedures followed the manufacturer's protocol. Four to five rats from each animal group were used, and all samples were run in duplicate. The range of the standard curve was 3–300 pg/ml, and a four-parameter logistic model was applied to fit the standard curve.

Messenger RNA Quantification

RNA Preparation. Frozen liver and uterus samples were ground into a fine powder under liquid nitrogen. Powdered samples were weighed, added to prechilled TRI Reagent (Invitrogen, Carlsbad, CA), and homogenized. Total RNA extractions were carried out using TRI Reagent and further purified by passage through RNeasy minicolumns (Qiagen, Valencia, CA) according to the manufacturer's protocols for RNA cleanup. The RNA concentrations were quantified spectrophotometrically (NanoDrop 2000c; Thermo Fisher Scientific, Waltham, MA), and purity and integrity were assessed by agarose-formaldehyde gel electrophoresis. All samples exhibited 260/280 absorbance ratios of approximately 2.0, and all showed intact ribosomal 28S and 18S RNA bands in an approximate ratio of 2:1 as visualized by ethidium bromide staining. Final total RNA preparations were diluted to desired concentrations (~25 ng/μL) in nuclease-free water (Ambion, Austin, TX) and stored in nuclease-free tubes at -80°C until use.

Quantification of mRNA Expression. The GILZ- and GR-specific quantitative real-time polymerase chain reaction (qRT-PCR) assays were developed and validated according to the Minimum Information for Publication of Quantitative Real-Time PCR Experiments (MIQE) guidelines (Bustin et al., 2009).

Both qRT-PCR assays involved use of *in vitro* transcribed cRNA standards, gene-specific TaqMan-based probes, and a single-step assay. An extensive description on the sub-cloning and construction of the *in vitro* transcribed cRNA standards was reported previously (Ayyar et al., 2015). Primer and probe sequences were designed and custom-synthesized (Biosearch Technologies, Novato, CA). The qRT-PCR was performed using a Brilliant qRT-PCR Core Reagent Kit, 1-Step (Stratagene, La Jolla, CA) in a Stratagene MX3005P thermocycler according to the manufacturer's instructions. Primer and probe sequences were as follows:

GR, forward primer 5′-AACATGTTAGGTGGGCGTCAA-3′,

GR, reverse primer 5′-GGTGTAAGTTTCTCAAGCCT AGTATCG-3’,

GR, FAM-labeled probe, 5′ TGATTGCAGCAGTGAAATGGGCAAAG-3′;

GILZ, forward primer 5’- GGAGGTCCTAAAGGAGCAGATTC- 3’,

GILZ, reverse primer 5’- GCGTCTTCAGGAGGG TATTCTC- 3’, and

GILZ, FAM-labeled probe, 5’-TGAGCTGGTTGAGAAGAACTCGCA- 3’

The concentrations of the primers, probes, and magnesium chloride were optimized, and the reaction conditions reported (Ayyar et al., 2015). A volume of 2.5 μL of total RNA (~ 62.5 ng/ μL) was used for each sample. Standards were run in duplicate and samples in triplicate; intra- and inter-assay CV were less than 20%. Additional reverse-transcriptase minus controls were included to ensure lack of DNA contamination in each sample.

Additional Data Source

The time-course of total plasma concentrations of 17β-estradiol across the four-day rat estrous cycle under 12 h daily light:dark cycles was obtained from Smith et al. (1975). The data in the report was obtained from female Sprague Dawley Rats weighing between 200 - 250 g, which was comparable to the body weights of the female Wistar rats used in our studies. Mean plasma concentrations of estradiol were extracted from published graphs in the report by computer digitization (WebPlotDigitizer, version 4.1, https://automeris.io/WebPlotDigitizer).

Systems PK/PD Modeling and Data Analysis

Pharmacokinetics

The concentration-time profiles of MPL in rats as modeled in Part II was incorporated into the current systems model. The mPBPK model equations and parameters describing the plasma and tissue concentrations of MPL in male and female rats were described (Ayyar et al., 2019a).

Mechanistic Basis for Pharmacodynamics

The series of steps controlling the signal transduction events for genomic CS actions along with the mechanism for the genome-level interaction of estrogens and CS are depicted in Fig. 1. Free (unbound) plasma concentrations of glucocorticoid hormones and synthetic CS rapidly distribute into intracellular spaces within tissues. Furthermore, systemic administration of CS results in an inhibition of endogenous CST secretion via a negative feedback loop on the HPA axis, resulting in time-dependent decreases in plasma CST concentrations. The unbound fractions of endogenous and exogenous steroids in tissues interact in a competitive manner with the cytosolic GR based on their relative receptor affinity. Binding of the steroids to its receptor produces an activated complex which rapidly translocates into the nucleus and binds specific GRE sites on target DNA. This process transcriptionally enhances or down-regulates the turnover rates of numerous target genes within a tissue, including GILZ. Circadian-driven production of endogenous CST and GR mRNA in rats produces non-stationarities in the receptor-mediated control of tissue gene expression (Hazra et al., 2007b; Almon et al., 2008). In addition to driving a rapid reduction in free cytosolic receptors by the translocation process, elevated cellular concentrations of CS induce a homologous down-regulation of their own receptors via decreased transcription, and consequent reductions in mRNA synthesis and free GR densities in the cytosol (Oakley and Cidlowski, 1993). After exerting their transcriptional effects, the steroid-receptor complexes in the nucleus may dissociate from GREs and return to the cytosol. Therefore, the total pool of free cytosolic GR constitutes a composite of recycled and *de novo* synthesized GR molecules.

Unbound plasma concentrations of E_2 in female rats can rapidly equilibrate within tissues (Puig-Duran et al., 1979) and interact with cytoplasmic ER. Activated ER complexes subsequently translocate into the nucleus and modulate its own target genes (Stossi et al., 2004) in a manner similar to CS. Cooperative binding of two different steroid hormone receptors at single target enhancer elements has been demonstrated (Tsai et al., 1989). In the presence of both CS and estrogens, GR and ER complexes in the nucleus can interact within the promoter regions of several CS-regulated target genes, including GILZ (Tynan et al., 2004; Whirledge et al., 2013). This mechanism for CS involves the recruitment of both GR and ER to a specific GRE site; for example, GRE site 1919-1794 in the promoter region of GILZ (Whirledge and Cidlowski, 2013). This interaction results in a competitive antagonism of CS gene regulation by E_2.

Mathematical Model

Figure 2 presents the scheme for the entire mPBPK/PD/PG model for MPL actions in male and female animals. The equations and parameters for modeling the dynamics of CST suppression were described in Part II and used unchanged in the expanded systems model. In the unperturbed system (i.e. no MPL exposure), the model operates under homeostatic (steady-state) conditions driven by circadian variations in endogenous CST concentrations.

Model Assumptions

Certain assumptions were made during the development of this mathematical model. 1) The endogenous time-course of E_2 across the four-day estrous cycle in female rats is unaltered upon bolus dosing of MPL, 2) ligand-induced down-regulation of the ER in tissues is negligible at physiological concentrations of E_2 and equilibrium binding conditions are operable, 3) influence of other sex hormones (e.g. progesterone), which are also elevated during PE is negligible (if existent) compared to E_2, 4) only the free fraction of E_2 (Montano et al., 1995; Plowchalk and Teeguarden, 2002) can interact with ER in tissues, and 5) the kinetic rate constants controlling GR mRNA and protein dynamics are independent of sex and tissue-type.

JPET Fast Forward. Published on June 13, 2019 as DOI: 10.1124/jpet.119.257543
This article has not been copyedited and formatted. The final version may differ from this version.

Mathematical Description of Model

Glucocorticoid Receptor Dynamics. The fifth-generation model of CS proposed by Ramakrishnan et al. (2002) and modified by Hazra et al. (2007) was adapted to incorporate the binding of endogenous CST to free cytosolic receptors in both sexes (under circadian homeostasis and in the presence of MPL). The differential equations and initial conditions (IC) for GR dynamics in the tissues are:

$$\frac{dGR}{dt} = k_{s,GR} \cdot GR_m - k_{d,GR} \cdot R - k_{on,MPL} \cdot f_{ut,i,MPL} \cdot C_{t,i} \cdot GR - k_{on,CST} \cdot f_{up,CST} \cdot CST \cdot GR + k_{re} \cdot R_f \cdot CR_N + k_{re} \cdot R_f \cdot DR_N \qquad GR(0) = GR_0 \qquad (1)$$

$$\frac{dCR}{dt} = k_{on,CST} \cdot f_{u,pCST} \cdot CST \cdot GR - k_t \cdot CR \qquad CR(0) = CR_0 \qquad (2)$$

$$\frac{dCR_N}{dt} = k_t \cdot CR - k_{re} \cdot CR_N \qquad CR_N(0) = CR_{N(0)} \qquad (3)$$

$$\frac{dDR}{dt} = k_{on,MPL} \cdot f_{u,hepMPL} \cdot C_{hep} \cdot GR - k_t \cdot DR \qquad DR(0) = 0 \qquad (4)$$

$$\frac{dDR_N}{dt} = k_t \cdot DR - k_{re} \cdot DR_N \qquad DR_N(0) = 0 \qquad (5)$$

$$NR_{N\_TOT} = DR_N + CR_N \qquad (6)$$

where *GR* is the free cytosolic receptor, *CR* and *DR* are the cytosolic receptors bound to *CST* and *MPL*, CR_N and DR_N are the nuclear translocated complex concentrations, and NR_{N_TOT} is the total concentration of steroid-receptor complex in the nucleus. The first-order rate constants include receptor synthesis ($k_{s,GR}$) and degradation ($k_{d,GR}$), translocation of the receptor complexes into the nucleus (k_t), the overall turnover of DRn return receptors to cytosol (k_{re}), as well as the second-order rate constants of hormone- and drug-receptor association ($k_{on,CST}$ and $k_{on,MPL}$). Part of NR_{N_TOT} may recycle back to the cytosol controlled by the rate constant $R_f \cdot k_{re}$, and the rest is degraded with a rate constant $(1 - R_f) \cdot k_{re}$. The total concentrations of MPL in a specific tissue compartment "*i*" and CST in plasma are given by $C_{t,i}$ and *CST*. The $f_{ut,i,MPL}$ and

$f_{up,CST}$ are the unbound fractions of MPL in tissue "*i*" and CST in plasma. The $f_{ut,i,MPL}$ is calculated as the ratio of the plasma unbound fraction of MPL ($f_{up,MPL}$) and the tissue-to-plasma partition coefficient ($K_{P,i}$) for tissue *i*.

The notations used in Eqs. 1-6 are important for PD models when multiple steroids are present. When no drug is present: $NR_{N\_TOT} = CR_N$. The parameters GR_0, CR_0, and $CR_{N(0)}$ are the concentrations of the GR, CST bound to receptor, and CST bound to receptor in the nucleus at time zero under baseline conditions at steady-state. The GR_0 were fixed to experimentally measured values in liver (476 fmol/mg protein) and uterus (290 fmol/mg protein) from untreated rats (Izawa et al., 1984; Hazra et al., 2007b). The steady-state values for $CR_{(0)}$ and $CR_{N(0)}$ at time zero were defined as:

$$CR_0 = \frac{k_{on,CST} \cdot f_{up,CST} \cdot CST(0) \cdot GR(0)}{k_t} \tag{7}$$

$$CR_{N(0)} = \frac{k_t \cdot CR(0)}{k_{re}} \tag{8}$$

Eq. (1) was solved under steady-state conditions to yield $k_{s,GR}$:

$$k_{s,GR} = \frac{k_{d,GR} \cdot GR(0) + k_{on,CST} \cdot f_{u,pCST} \cdot CST(0) \cdot GR(0) - (k_{re} \cdot R_f) \cdot CR_N(0)}{GR_m(0)} \tag{9}$$

The GR mRNA (GR_m) showed circadian oscillations in livers from male rats (Hazra et al., 2007b), which were described using an indirect response (IDR) model with the mRNA synthesized by a time-dependent synthesis rate ($k_{s,GRm(t)}$) and degraded by first-order rate constant ($k_{d,GRm}$) as follows:

$$\frac{dGR_m}{dt} = k_{s,GRm}(t) - k_{d,GRm} \cdot GR_m \qquad GR_m(0) = GR_{m(0)} \tag{10}$$

The time-dependent synthesis rate of hepatic GR mRNA [$k_{s,GRm,liver}(t)$] was described using a two harmonic function (Hazra et al., 2007b):

$$k_{s,GRm,liver}(t) = a_{0,GRm} \cdot k_{d,GRm} + \left(a_{1,GRm} \cdot k_{d,GRm} + \frac{2\pi b_{1,GRm}}{24}\right) \cdot cos\left(\frac{2\pi T}{24}\right)$$

JPET Fast Forward. Published on June 13, 2019 as DOI: 10.1124/jpet.119.257543
This article has not been copyedited and formatted. The final version may differ from this version.

$$+\left(b_{1,GRm}\cdot k_{d,GRm}+\frac{2\pi a_{1,GRm}}{24}\right)\cdot sin\left(\frac{2\pi T}{24}\right)+\left(a_{2,GRm}\cdot k_{d,GRm}+\frac{2\pi b_{2,GRm}}{12}\right)\cdot cos\left(\frac{2\pi T}{12}\right)$$

$$+\left(b_{2,GRm}\cdot k_{d,GRm}+\frac{2\pi a_{2,GRm}}{12}\right)\cdot sin\left(\frac{2\pi T}{12}\right) \quad (11)$$

where a_i and b_i are Fourier coefficients associated with the harmonic oscillations.

Suppression of GR mRNA expression by MPL in liver was described by a DR_N - mediated inhibition of $k_{s,GRm,liver}(t)$ and subsequent inhibition of $k_{d,GRm}$ by a transduction signal generated from DR_N to capture a liver-specific rebound phenomenon,

$$\frac{dTC_1}{dt}=\frac{1}{\tau_{GRm}}\cdot(DR_N-TC_1) \quad (12)$$

$$\frac{dTC_2}{dt}=\frac{1}{\tau_{GRm}}\cdot(TC_1-TC_2) \quad (13)$$

$$\frac{dGR_{m,liv,mpl}}{dt}=k_{s,GRm,liver}(t)\cdot\left(1-\left(\frac{DR_N}{DR_N+IC_{50,GRm}}\right)\right)-k_{d,GRm}\cdot\left(1-\left(\frac{TC_2}{TC_2+IC_{50,TC_2}}\right)\right)\cdot GR_{m,liv,mpl} \qquad GR_{m,liv,mpl}(0)=GR_{m,liv.mpl(0)} \quad (14)$$

where TC_1 and TC_2 are two transit compartments, τ_{GRm} is the mean transit time for signal transduction from DR_N, $IC_{50,GRm}$ is the concentration of DR_N at which the synthesis rate of GR mRNA is reduced to 50% of its baseline, and $IC_{50,TC2}$ is the concentration of TC_2 responsible for 50% inhibition of the loss rate for GR mRNA.

Suppression of GR mRNA expression by MPL in uterus is given by:

$$\frac{dGR_{m,ut,mpl}}{dt}=k_{s,GRm,ut}\cdot\left(1-\left(\frac{DR_N}{DR_N+IC_{50,GRm}}\right)\right)-k_{d,GRm}\cdot GR_{m,ut,mpl} \qquad GR_{m,ut,mpl}(0)=GR_{m,ut,mpl(0)} \quad (16)$$

Because stationarity is assumed, $k_{s,GRm,ut}$ was defined as:

$$k_{s,GRm,ut}=k_{d,GRm}\cdot GR_{m,ut}(0) \quad (17)$$

JPET Fast Forward. Published on June 13, 2019 as DOI: 10.1124/jpet.119.257543
This article has not been copyedited and formatted. The final version may differ from this version.

The dynamics of GR mRNA has been previously assessed in liver, adipose, lung, and muscle from intact male rats (Hazra et al., 2007b; Sukumaran et al., 2011; Ayyar et al., 2017) and free cytosolic receptor densities in livers of male rats (Hazra et al., 2007b). While time-dependent down-regulation of receptor mRNA was observed in all tissues following MPL, a rebound in GR mRNA was observed specifically in male livers (Hazra et al., 2007b). It was assumed that hepatic GR mRNA followed a similar temporal pattern in female rat livers. Parameter values for hepatic receptor dynamics were employed to simulate receptor dynamics in the rat uterus (no rebound process was incorporated). Corrections for sex and/or tissue differences in baseline receptor mRNA [$GR_{m(0)}$] were made using measurements in control animals from each group. In addition, free receptor concentrations in the uterus of untreated rats (GR_0) was obtained from a previous study (Izawa et al., 1984).

Plasma Estradiol Concentrations. Endogenous concentrations of plasma E_2 vary significantly across the four-day estrous cycle in rodents. The profile for plasma E_2 in control (non-dosed) female rats was obtained from Smith et al. (1975). An empirical function (mimicking two joint Gaussian normal distribution curves) was constructed to approximate the time-course of plasma E_2 [$E_2(t)$]. The equation was fit to the experimental data and subsequently extended to repeat for a second cycle:

$$E_2(t) = BL + A \cdot e^{-\frac{(T-T_{pk1})^2}{\propto}} + B \cdot e^{-\frac{(T-T_{pk2})^2}{\beta}} + A \cdot e^{-\frac{\left(T-(\tau+T_{pk1})\right)^2}{\propto}} + B \cdot e^{-\frac{\left(T-(\tau+T_{pk2})\right)^2}{\beta}} \qquad (18)$$

where BL is the baseline concentration of plasma E_2, T is the actual time, the terms T_{pk1} and T_{pk2} represent the times of peak concentrations within the metestrus/diestrus and PE phases, A and B are the amplitudes of the first and second peak, α and β are fitting coefficients for the two peaks, and τ is the duration of one estrous cycle (96 h). Plasma concentrations of E_2 as described by Eq. (17) was used as an input to drive subsequent ER binding dynamics in liver and uterus.

Estrogen Receptor Binding. Plasma E_2 concentrations Eq. (17) were converted to nanomolar units and the free concentrations of E_2 in plasma ($C_{f,E2}$) were assumed to equilibrate with the intracellular spaces

JPET Fast Forward. Published on June 13, 2019 as DOI: 10.1124/jpet.119.257543
This article has not been copyedited and formatted. The final version may differ from this version.

(i.e., diffusion is not rate limiting) where the cytosolic ER is present. The concentration of cytosolic drug–receptor complex (ER_B) is given by:

$$ER_B = \frac{B_{max,ER} \cdot C_{f,E2}}{K_{D,E2} + C_{f,E2}} \quad (19)$$

where $C_{f,E2} = f_{up,E2} \cdot E_2(t)$, $B_{max,ER}$ is the total concentration of estrogen receptors, and $K_{D,E2}$ is the equilibrium dissociation constant. The values of $B_{max,ER}$ and $K_{D,E2}$ in rat liver and uterus were obtained from the literature (Notides, 1970; Aten et al., 1978; Branham et al., 2002; Plowchalk and Teeguarden, 2002). The bound hormone–receptor complex translocates into the cell nucleus and the rate of change of activated nuclear complex concentrations (ER_N) can be described as:

$$\frac{dER_N}{dt} = k_t \cdot (ER_B - ER_N) \qquad ER_{N(0)} = ER_{B(0)} \quad (20)$$

The value of k_t was assumed to be the same as used for describing nuclear translocation of the GR complex.

GILZ mRNA Dynamics. The transcriptional enhancement of GILZ mRNA synthesis by MPL has been described in various tissues from male rats (Ayyar et al., 2017). The expression of GILZ shows non-stationary baselines over time in multiple tissues with a pattern entrained to endogenous CST production in male rats (Ayyar et al., 2017). The dynamics of GILZ mRNA in both sexes was driven by NR_{N_TOT}, where circadian rhythms in gene expression would be expected to follow a pattern of CR_N in the absence of MPL, whereas the receptor-mediated enhancement of GILZ would occur in a competitive manner in the presence of endogenous and exogenous agonists (Ariëns et al., 1957). Based upon the genomic mechanism of interaction of nuclear steroid-receptor complexes (Whirledge and Cidlowski, 2013), it is assumed that the ER_N in tissues interact with NR_{N_TOT} by competing for binding at the same site of the GILZ promoter region, resulting in competitive antagonism of GILZ enhancement. Consistent with this mechanism, the proposed equation accounts for antagonist pharmacology (Gaddum, 1957) via a nuclear ER concentration-dependent increase in the apparent SC_{50} of the nuclear GR complex:

JPET Fast Forward. Published on June 13, 2019 as DOI: 10.1124/jpet.119.257543
This article has not been copyedited and formatted. The final version may differ from this version.

$$\frac{dGILZ_m}{dt} = k_{s,GILZm} \cdot \left[1 + \left(\frac{S_{max} \cdot NR_{N\_TOT}}{SC_{50,GILZm} \cdot \left(1 + \frac{ER_N}{K_i}\right) + NR_{N\_TOT}}\right)\right] - k_{d,GILZm} \cdot GILZ_m \quad (21)$$

where $k_{s,GILZm}$ is the zero-order synthesis rate and $k_{d,GILZm}$ the first-order degradation rate constant for GILZ mRNA, S_{max} is the maximal stimulatory capacity for GILZ synthesis by NR_{N_TOT}, $SC_{50,GILZm}$ is the concentration of NR_{N_TOT} producing half-maximal stimulation of GILZ mRNA, and K_i (inhibition constant) is the nuclear ER complex (ER_N) concentration producing 50% inhibition of NR_{N_TOT} - mediated enhancement of GILZ. The $k_{s,GILZm}$ at steady-state is:

$$k_{s,GILZm} = \frac{k_{d,GILZm} \cdot GILZ_m(0)}{1 + \left(\frac{S_{max} \cdot NR_{N\_TOT}}{SC_{50,GILZm} \cdot \left(1 + \frac{ER_N}{K_i}\right) + NR_{N\_TOT}}\right)} \quad (22)$$

Data Analysis

Statistical Analysis. Data were analyzed statistically by Student's t-tests using SigmaPlot 14.0 (Systat Inc., San Jose, CA), and $p < 0.05$ was considered to be statistically significant.

PK/PD Data Analysis. The ADAPT 5 software was used for implementing the systems model, including data fitting and simulation of model equations (D'Argenio et al., 2009). The maximum likelihood method was applied for fitting the data. Replicate data at each time point from animals in each experiment were pooled. The goodness of fit was assessed by system convergence, visual inspection of the fitted curves, improved likelihood, examination of residuals, and precision (CV%) of the estimated parameters. The following variance model was specified for the PD outputs:

$$V_i = V(\theta, \sigma, t) = [\sigma_1 \cdot Y(\theta, t_i)]^{\sigma_2} \quad (23)$$

where V_i is the variance of the ith data point, σ_1 and σ_2 are the variance parameters, and *Yi* is the model predicted response. Variance parameters σ_1 and σ_2 were estimated (or σ_2 was fixed to 2) along with model parameters during fittings. Area under the effect curve (*AUEC*) values for observed and model-fitted data

were calculated using the linear-up log-down trapezoidal method and compared using Phoenix 8.1 (Certara Corporation, Princeton, NJ).

All circadian as well as PK/PD data were interpreted and modeled across the time scale of the rodent reproductive cycle (i.e. four days) starting at 12:00 AM on Day 1 (E phase) with female rats. Drug was administered between 1.5 and 3 hours after lights ON in males ("Day 1"), females within the E phase (Day 1), and in females within the PE phase (Day 4). For simplicity, the dosing time was assumed to be at circadian time 2.5 hours for all rats. In the females, dosing therefore occurred at 8.5 hours (6 hours of dark + 2.5 hours after lights ON) after entering a new phase of the cycle. The same was assumed for males to ensure consistency across groups (although reproductive cycles are irrelevant in the males; stable baseline E_2 concentrations assumed). Time-course data from males, E-, and PE-phased female rats were fitted jointly using a single systems model. To ensure that a steady-state in all PD profiles was achieved following dosing within E on Day 1 and prior to modeling PE, MPL was re-inputted into the system on Day 8 (i.e. second PE) for the PE female group. Hence, all PD profiles are plotted and modeled with respect to estrous time, with MPL given at 8.5 hours in males and E females, and at 176.5 hours in PE females.

Results

Glucocorticoid Receptor Dynamics.

Baseline hepatic GR mRNA was compared between males aged 7 weeks (Cohort 4) and 11 weeks (Cohort 5). No differences were observed (Supplemental Figure 1). Hepatic GR mRNA between males (Cohort 5) and E females (Cohort 1) was compared at baseline and at 4 h after MPL dosing. As expected, ~ 50% down-regulation in GR mRNA occurred at 4 h after MPL compared to baseline in both sexes (Fig. 3). There was no statistically significant difference in hepatic GR mRNA at baseline and after MPL (Fig. 3) in both groups, consistent with previous findings in liver at the mRNA and protein levels (Duma et al., 2010). Therefore, identical receptor concentrations and kinetic rate constants as obtained from fitting hepatic GR mRNA and free cytosolic receptor data in males were assumed in both sexes (note: sex-specific PK and unbound plasma CST concentrations were used to drive receptor dynamics). This assumption was further confirmed, in part, by comparative time-course measurements of hepatic GR mRNA in males and E females up to 24 h after MPL (Supplemental Figure 2). Next, uterine expression of GR mRNA was assessed in E (Cohort 1) and PE (Cohort 2) females at baseline and at 4 h after dosing. Similar to liver patterns, mRNA expression was ~50% decreased by 4 h after dosing compared to baseline within both groups, with no significant differences in baseline or suppression across both groups.

The dynamics of hepatic GR mRNA in male rats (Hazra et al., 2007b) after MPL dosing along with the model fittings are shown in Fig 4. MPL caused significant perturbation in GR mRNA, which unlike the profiles for CST (Ayyar et al., 2019a), displayed a rebound phenomenon in this tissue before slowly returning to its regular daily rhythm beyond 72 h. The down-regulation as well as rebound phase was captured suitably well. The time course of free hepatic cytosolic receptor density in male rats (Hazra et al., 2007b) along with the model fittings are shown in Fig. 4. The developed model, which extended the model of Hazra et al. (2007) to include competitive CST binding, captured the free receptor profiles reasonably well. All parameter values governing GR mRNA and receptor dynamics controlled by MPL were assumed to be the same for CST and were fixed based on Hazra et al. (2007). Estimation of the

JPET Fast Forward. Published on June 13, 2019 as DOI: 10.1124/jpet.119.257543
This article has not been copyedited and formatted. The final version may differ from this version.

parameter $k_{on,CST}$ yielded values with low precision (high % CV), likely due to model over-parameterization in the absence of non-stationary baseline receptor data. Using the obtained kinetic parameters in liver, simulations of GR mRNA and receptors in uterus from E and PE females were performed after correction for tissue differences in GR mRNA (from Fig. 3) and cytosolic receptor concentrations (Izawa et al., 1984) (Supplemental Figure 3). The uterine GR mRNA data at 4 h was well predicted by the model in both groups. In the absence of extended time-course and circadian GR data in uterus, no rebound in GR mRNA as well as a stable baseline was assumed.

Plasma Estradiol and Tissue Receptor Occupancy.

Plasma concentrations of E_2 were assayed in a group of non-dosed female rats within either the E (n = 4) or PE (n = 4) stages (blood samples were taken at 3 h in PE females and between 2-6 h after lights ON in E females). As depicted in Fig. 5 (left panel), plasma E_2 concentrations were significantly elevated in PE (19.6 ± 5.9 ng/mL) compared to E (2.0 ± 0.48 ng/mL). A similar trend was demonstrated by Smith et al. (1975), but their study followed plasma concentrations of 17β-E_2 more extensively over the entire course of the rat estrous cycle. Figure 5 (middle panel) depicts the profile of plasma E_2 over 4 days in the female rat along with its mathematical characterization. Plasma E_2 was stable throughout the E phase (~ 6.9 ng/mL), but showed a sharp rise during PE to peak concentrations of ~ 39 ng/mL. Since the model assumed that the hormonal profiles in females were not perturbed by drug, an empirical function was constructed to approximate the time-course of plasma E_2 that reasonably well captured the data. Total E_2 was corrected for plasma protein binding to albumin (Plowchalk and Teeguarden, 2002) and the free concentrations of E_2 were subsequently used to drive ER binding in the cytosol and subsequent ER_N concentrations in liver and uterus (Fig. 5; right panel). The simulations indicated higher occupancy and amounts of ER_N in uterus compared to liver, largely attributable to a higher ER density in uterus (560 fmol/mg protein) compared with liver (24.5 fmol/mg protein). Parameter values for ER binding are listed in Table 2, along with their literature sources.

JPET Fast Forward. Published on June 13, 2019 as DOI: 10.1124/jpet.119.257543
This article has not been copyedited and formatted. The final version may differ from this version.

GILZ mRNA Dynamics.

Liver. The PD enhancement profiles of hepatic GILZ mRNA by MPL in males and females, along with the model fitted profiles and simulated driving forces, are shown in Figure 6. The developed model was able to jointly capture the data quite well. Table 3 lists parameter values that were either fixed or estimated from the fitting. Figure 6 (top left) displays the time-course of enhancement of hepatic GILZ mRNA by MPL in male rats along with the model fits. The enhancement profile of GILZ mRNA was nearly identical across both male studies (Cohorts 4 and 5; comparison not shown). In males, GILZ increased very rapidly from the baseline (1893 ± 423 molecules/ng RNA) to the peak (7867 ± 1821 molecules/ng RNA) by 0.75 h after dosing. The model-fitted profile showed a return to baseline around 24 h in males, with GILZ mRNA displaying modest circadian rhythmicity in expression (driven by endogenous CST concentrations). The PD profiles of hepatic GILZ message in E and PE females are shown in Fig. 6 (top right). GILZ, in general, showed higher peak expression, a more prolonged return profile, and a resultant 2.5 to 3-fold increase in *AUEC* in females, regardless of estrous stage, compared to males (Table 4). The model jointly captured the observed sex differences fairly well, although peak responses were somewhat under-predicted in both groups. The estimated first-order degradation rate-constant of GILZ mRNA in liver ($k_{deg,GILZm}$) value of 7.5 h^{-1} (21.8 % CV) was significantly higher compared to estimates in other tissues, including lung, muscle, and adipose (Ayyar et al., 2017), as reflected by the profile of GILZ mRNA in liver. The extent and pattern of up-regulation of hepatic GILZ mRNA in all groups (Fig. 6; bottom left) corresponded with that of the nuclear steroid-receptor complex (Fig. 6; bottom right).

Uterus. The PD enhancement profiles of GILZ mRNA by MPL in uterus from E and PE females, along with model fitted profiles, are shown in Figure 7. The model captured the dynamics of GILZ in both groups reasonably well. Parameter estimates are listed in Table 3. Baseline expression of uterine GILZ mRNA was significantly lower in PE (2400 ± 727 molecules/ng RNA) compared to E (3245 ± 548 molecules/ng RNA), and correlated inversely to plasma estradiol concentrations in both estrous phases (Fig. 5), suggestive of antagonism of uterine GILZ mRNA even in the absence of drug. Uterine GILZ

JPET Fast Forward. Published on June 13, 2019 as DOI: 10.1124/jpet.119.257543
This article has not been copyedited and formatted. The final version may differ from this version.

mRNA was enhanced to a greater extent in E compared to PE females, indicated by a higher peak response (13476 ± 489 vs. 7167 ± 2528 molecules/ng RNA molecules/ng RNA) and baseline-corrected *AUEC* values (Table 4) in E compared to PE. The proposed model captured the trends of both groups quite well (Fig. 7 and Table 4), although the peak of response was under-predicted. The estimated $k_{deg,GILZm}$ value in uterus of 1.9 h^{-1} (27.5 %CV) was considerably lower compared to liver, yet 4-6 fold higher compared to other tissues (Ayyar et al., 2017), indicating a pronounced inter-tissue variability for this parameter. The SC_{50} for GILZ message enhancement by MPL was reasonably similar in liver (558 fmol/mg protein; 5.5 %CV) and in uterus (672 fmol/mg protein; 19.2 %CV). A common S_{max} value of 7.5 (Hazra et al., 2008) suitably described the dynamics of GILZ mRNA across all tissues and both sexes. The value for K_i estimated based on fitting of the uterine data was 61.4 fmol/mg protein (68.6 %CV). These results collectively support the hypothesis of an estrogen-mediated antagonism of receptor/gene-mediated MPL PD. Joint characterization of both data sets upon removing the antagonistic regulation by ER_N from Eq. (22) led to a systematic over-prediction of uterine GILZ mRNA dynamics in PE females (not shown).

Discussion

This work represents a continuation of our long-standing efforts to decipher the complex pharmacogenomic mechanisms by which glucocorticoids regulate body functions *in vivo*. Previous generation mechanistic PK/PD models were built upon experimental studies conducted in ADX male rats, and later extended to intact male rats. The current work examined the dynamic effects of CS in female rats, a more physiologically complex, however, equally relevant preclinical animal model. Several factors, related to PK and PD, needed careful attention due to complexities arising from 24-hour circadian rhythms as well as longer 96-hour reproductive rhythms. Despite added complications associated with use of female rats, our objective was to quantitatively understand the interplay of endogenous glucocorticoid hormones, exogenous CS, and sex hormones employing a systems PK/PD modeling approach.

Studies examining the variability in drug response should consider factors influencing variability in drug exposure in relevant biophases (Mager and Kimko, 2016). *In vitro* properties of MPL PK (Ayyar et al., 2019b) as well as *in vivo* sex differences in plasma and tissue PK of MPL (Ayyar et al., 2019a) were investigated and accounted for in both sexes using an extended mPBPK modeling approach. Endogenous agonists contribute to PD variability in drug responses (Levy, 1998). The model incorporated sex- and estrous-phase dependent differences in the circadian concentrations of CST (Atkinson and Waddell, 1997), as well as the rapid adrenal suppressive effects of MPL (Ayyar et al., 2019a). Differences (or lack thereof) in cytosolic receptor concentrations in rat livers and uterus were accounted for using experimental measurements from the literature (Izawa et al., 1984; Hazra et al., 2007b; Duma et al., 2010) with kinetic parameters controlling GR dynamics held constant in all systems. In ER-expressing human uterine epithelial cells, the presence of low concentrations (1-10 pM) of E_2 produced interactions between the activated ER and GR complexes, resulting in an antagonism of CS-inducible GILZ (Whirledge and Cidlowski, 2013). We estimated that endogenous concentrations of unbound plasma E_2 would rise to ~7.5 pM by the peak of PE, well within the antagonistic range reported *in vitro*. Of translational and

physiological relevance, we hypothesized that such drug-hormone interactions would contribute to time-sex-dependent variability in genomic MPL actions as a function of estrous rhythms.

A quantitative systems approach was used to understand the dynamic mechanisms controlling sex- and tissue-specific MPL actions. Previous generation models assumed that the kinetics of drug distribution into tissues was not rate-limiting (i.e. well perfused entry), and that unbound concentrations of MPL in plasma interacted with cytosolic receptors (Hazra et al., 2007a). Here, total MPL concentrations were measured in liver in both sexes (Ayyar et al., 2019a), the unbound tissue fraction was calculated under assumption of the "free hormone" hypothesis (Mendel, 1989), and free drug concentrations in liver were used to drive receptor binding. The time-course of hepatic free cytosolic receptor data in males was well captured using this model despite employing the parameter values for receptor kinetics estimated upon assuming free plasma MPL as the driving force (Hazra et al., 2007b), indicating that prior model assumptions regarding the rapid equilibration kinetics of MPL in liver are maintained. It is possible that the unbound liver fraction ($f_{u,hep}$) represents an "apparent" value since active transport processes may contribute to hepatic uptake of MPL (Lackner et al., 1998; Ayyar et al., 2019b).

To realize circadian oscillations in hepatic tyrosine aminotransferase (TAT) dynamics, a previous model (Hazra et al., 2007b) assumed equilibrium binding of CST to receptors as a distinct process independent of MPL kinetics and GR engagement. The present model built upon this concept but incorporated competitive binding for free cytosolic receptors by drug and hormone, thus introducing non-stationarity in steroid pharmacogenomics through a coupled process. Estimation of the parameter $k_{on,CST}$ yielded values with low precision (high % CV), likely due to model over-parameterization in the absence of non-stationary baseline receptor data. To address this issue, a local sensitivity analysis of this parameter was employed during the model building process. Specifically, $k_{on,CST}$ was varied by 100-fold across a physiologically-plausible range and fixed to an estimate (0.001 $nM^{-1} \cdot h^{-1}$) which was ~ 16-fold lower compared to that of MPL, and provided optimal characterization of the data. Further experimental testing of CST binding kinetics is needed to confirm the accuracy of this model-based value. It was assumed that kinetic rate-constants and PD parameters governing the profiles of GR and its mRNA were

identical across sex- and tissue-type. While more extensive receptor data in tissues in both sexes would ascertain the validity of these assumptions, the model was able to generate hepatic nuclear complex profiles that corresponded reasonably well with the extents and patterns of hepatic GILZ mRNA in both sexes. Following the same assumptions, uterine GILZ mRNA profiles were also captured reasonably well. Nonetheless, one possible reason for the under-estimation of peak GILZ responses in females could relate to modest differences in receptor dynamics.

Baseline GILZ mRNA at time of dosing was higher in PE (2538 molecules/ng RNA) compared to E and in males (1893 and 2051 molecules/ng RNA), possibly attributable to elevated plasma CST concentrations in PE (~143 ng/mL) compared to E and males during that time (~32 ng/mL) (Ayyar et al., 2019a). Model-based simulations revealed that inclusion of CST dynamics produced circadian rhythmicity in NR_{N_TOT} after drug washout (Fig 6; bottom right), consequently producing a characteristic circadian pattern in tissue GILZ mRNA (Ayyar et al., 2017); one which followed the pattern of plasma CST in a delayed manner. Unlike in liver, baseline GILZ mRNA in uterus was significantly lower in PE (2400 molecules/ng RNA) compared to E females (3245 molecules/ng RNA) despite higher plasma CST concentrations. This is likely attributable to the antagonistic effects on basal GILZ mRNA produced by an elevated occupancy of ER in uterus during PE (Fig. 5; right panel). Therefore, particular attention was needed to discern whether or not the lower enhancement of GILZ mRNA by MPL during PE was explained solely by a lower baseline (Sun and Jusko, 1999). Upon modeling uterine GILZ enhancement by MPL in the absence and presence of antagonism, it was evident that inclusion of antagonism by ER_N on basal and drug-regulated GILZ enhancement (Eq. 22) most suitably described the totality of data. Although the $k_{deg,GILZm}$ was same in both sexes, it was interesting to find a pronounced inter-tissue variability in this parameter across liver and uterus, consistent with previous findings (Ayyar et al., 2017). Similar observations of a ‘systems variability’ in the degradation rate-constants for some signaling proteins across several lines of multiple myeloma cells was recently reported (Ramakrishnan and Mager, 2018).

The *AUEC* of hepatic GILZ enhancement was significantly higher in females compared to males (Fig. 6 and Table 4), controlled by PK-driven increases in hepatic DR_N concentrations (Fig. 6) in females. Examination of GILZ response in two distinct tissues (liver and uterus) and two distinct estrous phases (E and PE) in females, however, revealed estrous cycle- and ER-dependence in the post-receptor control of genomic MPL action. In liver – a tissue of relatively low ER (Table 2), there was a negligible influence of E_2-ER signaling, as evidenced by the nearly identical profiles of hepatic GILZ mRNA between E and PE females. In contrast, in uterus – a tissue with high ER content (Table 2), the *AUEC* of GILZ up-regulation was significantly lower in PE compared to E females (Table 4) despite no PK or receptor differences, providing *in vivo* support to the hypothesis of an ER_N-mediated antagonism of MPL-regulated GILZ.

The ability of the proposed systems model to jointly capture genomic GILZ enhancement by MPL across sex, tissues, and (circadian and estrous) time is encouraging and has several implications. First, reasonable prediction of GILZ mRNA dynamics across all the groups justify the assumption of identical kinetic rate constants for GR dynamics across sex and tissues. Second, the development of a systems model platform enabled a separation and systematic examination of drug- and system-specific parameters and their relative contributions in limiting the overall genomic response to MPL dosing. Third, the results suggest that the principle drug-specific determinants of receptor/gene-mediated MPL response remain its PK and receptor affinity, whereas tissue GR and ER content, endogenous E_2 concentrations, and biomarker turnover represent system-specific factors influencing steroid response.

It should be recognized that the estrous cycle regulates not only E_2 but also other sex hormones such as progesterone and prolactin (Smith et al., 1975). The role of progesterone as a contributor to sex differences in PD responses (e.g. QT prolongation) has been reviewed (Sedlak et al., 2012). The potential roles of testosterone, progesterone, and other sex hormones in interacting with glucocorticoid signaling requires further examination. The current work examined sex hormone effects within a physiological range. Our present findings provide a basis for further examination of MPL-regulated pharmacogenomics under exogenous E_2 administration using the ovariectomized (OVX) rat model. Such a study design could 1) clarify the disposition kinetics and exposure of E_2 at the biophase, 2) permit evaluation of potential PK

interactions between MPL and E_2, 3) provide a broader characterization of the concentration-dependent antagonistic relationship in PD, and 4) yield robust data to challenge predictions based upon the current model.

In conclusion, differences in PK and receptor-mediated PD of MPL were identified based on sex, estrous stage, and tissue type. The time-course of MPL actions were interpreted within the context of 24-hour circadian biorhythms as well as 4-day reproductive biorhythms. The developed model offers a mechanistic platform to integrate and evaluate the determinants of sex- and tissue-specificity in CS actions. This mechanistic systems model may also form the basis for explaining the interactions of E_2 with other drugs and xenobiotics acting via nuclear receptors.

Authorship contributions

Participated in research design: Ayyar, DuBois, Almon, Jusko

Conducted experiments: Ayyar, DuBois

Performed data analysis*:* Ayyar, Jusko

Wrote or contributed to the writing of the manuscript: Ayyar, DuBois, Almon, Jusko

REFERENCES

Almon RR, Yang E, Lai W, Androulakis IP, Ghimbovschi S, Hoffman EP, Jusko WJ and Dubois DC (2008) Relationships between circadian rhythms and modulation of gene expression by glucocorticoids in skeletal muscle. *Am J Physiol Regul Integr Comp Physiol* **295**:R1031-1047.

Ariëns EJ, van Rossum JM and Simonis AM (1957) Affinity, intrinsic activity and drug interactions. *Pharmacol Rev* **9**:218-236.

Aten RF, Dickson RB and Eisenfeld AJ (1978) Estrogen receptor in adult male rat liver. *Endocrinology* **103**:1629-1635.

Atkinson HC and Waddell BJ (1997) Circadian variation in basal plasma corticosterone and adrenocorticotropin in the rat: Sexual dimorphism and changes across the estrous cycle. *Endocrinol* **138**:3842-3848.

Ayroldi E and Riccardi C (2009) Glucocorticoid-induced leucine zipper (GILZ): a new important mediator of glucocorticoid action. *FASEB J* **23**:3649-3658.

Ayyar VS, Almon RR, Jusko WJ and DuBois DC (2015) Quantitative tissue-specific dynamics of in vivo GILZ mRNA expression and regulation by endogenous and exogenous glucocorticoids. *Physiol Rep* **3**:e12382.

Ayyar VS, DuBois DC, Almon RR and Jusko WJ (2017) Mechanistic multi-tissue modeling of glucocorticoid-induced leucine zipper regulation: Integrating circadian gene expression with receptor-mediated corticosteroid pharmacodynamics. *J Pharmacol Exp Ther* **363**:45-57.

Ayyar VS, DuBois DC, Almon RR and Jusko WJ (2019a) Modeling corticosteroid pharmacokinetics and pharmacodynamics – II: Sex differences in methylprednisolone pharmacokinetics and corticosterone suppression. *Accepted*.

Ayyar VS, Song D, DuBois DC, Almon RR and Jusko WJ (2019b) Modeling corticosteroid pharmacokinetics and pharmacodynamics – I: Determination and prediction of dexamethasone and methylprednisolone tissue binding in the rat. *Accepted*.

Ayyar VS, Sukumaran S, DuBois DC, Almon RR, Qu J and Jusko WJ (2018) Receptor/gene/protein-mediated signaling connects methylprednisolone exposure to metabolic and immune-related pharmacodynamic actions in liver. *J Pharmacokinet Pharmacodyn* **45**:557-575.

Branham WS, Dial SL, Moland CL, Hass BS, Blair RM, Fang H, Shi L, Tong W, Perkins RG and Sheehan DM (2002) Phytoestrogens and mycoestrogens bind to the rat uterine estrogen receptor. *J Nutr* **132**:658-664.

Bustin SA, Benes V, Garson JA, Hellemans J, Huggett J, Kubista M, Mueller R, Nolan T, Pfaffl MW, Shipley GL, Vandesompele J and Wittwer CT (2009) The MIQE guidelines: Minimum information for publication of quantitative real-time PCR experiments. *Clin Chem* **55**:611-622.

D'Argenio D, Schumitzky A and Wang X (2009) ADAPT 5 user's guide: Pharmacokinetic/pharmacodynamic systems analysis software, in, BioMedical Simulations Resource, Los Angeles.

Dickson RB and Eisenfeld AJ (1979) Estrogen receptor in liver of male and female rats: Endocrine regulation and molecular properties. *Biol Reprod* **21**:1105-1114.

Duma D, Collins JB, Chou JW and Cidlowski JA (2010) Sexually dimorphic actions of glucocorticoids provide a link to inflammatory diseases with gender differences in prevalence. *Sci Signal* **3**:ra74.

Gaddum JH (1957) Theories of drug antagonism. *Pharmacol Rev* **9**:211-218.

Hazra A, DuBois DC, Almon RR and Jusko WJ (2007a) Assessing the dynamics of nuclear glucocorticoid-receptor complex: adding flexibility to gene expression modeling. *J Pharmacokinet Pharmacodyn* **34**:333-354.

Hazra A, DuBois DC, Almon RR, Snyder GH and Jusko WJ (2008) Pharmacodynamic modeling of acute and chronic effects of methylprednisolone on hepatic urea cycle genes in rats. *Gene Regul Syst Bio* **2**:1-19.

Hazra A, Pyszczynski N, DuBois DC, Almon RR and Jusko WJ (2007b) Modeling receptor/gene-mediated effects of corticosteroids on hepatic tyrosine aminotransferase dynamics in rats: Dual regulation by endogenous and exogenous corticosteroids. *J Pharmacokinet Pharmacodyn* **34**:643-667.

Izawa M, Satoh Y, Iwasaki K and Ichii S (1984) Glucocorticoid receptor in the rat uterus. *Endocrinol Jpn* **31**:491-500.

Jusko WJ (1995) Pharmacokinetics and receptor-mediated pharmacodynamics of corticosteroids. *Toxicology* **102**:189-196.

Kuiper GG, Carlsson B, Grandien K, Enmark E, Haggblad J, Nilsson S and Gustafsson JA (1997) Comparison of the ligand binding specificity and transcript tissue distribution of estrogen receptors alpha and beta. *Endocrinology* **138**:863-870.

Lackner C, Daufeldt S, Wildt L and Allera A (1998) Glucocorticoid-recognizing and -effector sites in rat liver plasma membrane. Kinetics of corticosterone uptake by isolated membrane vesicles. III. Specificity and stereospecificity. *J Steroid Biochem Mol Biol* **64**:69-82.

Levy G (1998) Predicting effective drug concentrations for individual patients. Determinants of pharmacodynamic variability. *Clin Pharmacokinet* **34**:323-333.

Mager DE and Kimko HHC (2016) Systems Pharmacology and Pharmacodynamics: An Introduction, in *Systems Pharmacology and Pharmacodynamics* (Mager DE and Kimko HHC eds) pp 3-14, Springer International Publishing, Cham (Switzerland).

Mager DE, Pyszczynski NA and Jusko WJ (2003) Integrated QSPR--pharmacodynamic model of genomic effects of several corticosteroids. *J Pharm Sci* **92**:881-889.

Mendel CM (1989) The free hormone hypothesis: a physiologically based mathematical model. *Endocr Rev* **10**:232-274.

Montano MM, Welshons WV and vom Saal FS (1995) Free estradiol in serum and brain uptake of estradiol during fetal and neonatal sexual differentiation in female rats. *Biol Reprod* **53**:1198-1207.

Nichols AI, Boudinot FD and Jusko WJ (1989) Second generation model for prednisolone pharmacodynamics in the rat. *J Pharmacokinet Biopharm* **17**:209-227.

Notides AC (1970) The binding affinity and specificity of the estrogen receptor of the rat uterus and anterior pituitary. *Endocrinology* **87**:987-992.

Oakley RH and Cidlowski JA (1993) Homologous down regulation of the glucocorticoid receptor: the molecular machinery. *Crit Rev Eukaryot Gene Expr* **3**:63-88.

Plowchalk DR and Teeguarden J (2002) Development of a physiologically based pharmacokinetic model for estradiol in rats and humans: a biologically motivated quantitative framework for evaluating responses to estradiol and other endocrine-active compounds. *Toxicol Sci* **69**:60-78.

Puig-Duran E, Greenstein BD and MacKinnon PC (1979) The effects of serum oestrogen-binding components on the unbound oestradiol-17 beta fraction in the serum of developing female rats and on inhibition of [3H]oestradiol uptake by uterine tissue in vitro. *J Reprod Fertil* **56**:707-714.

Ramakrishnan R, DuBois DC, Almon RR, Pyszczynski NA and Jusko WJ (2002) Fifth-generation model for corticosteroid pharmacodynamics: application to steady-state receptor down-regulation and enzyme induction patterns during seven-day continuous infusion of methylprednisolone in rats. *J Pharmacokinet Pharmacodyn* **29**:1-24.

Ramakrishnan V and Mager DE (2018) Pharmacodynamic models of differential bortezomib signaling across several cell lines of multiple myeloma. *CPT Pharmacometrics Syst Pharmacol*:[Epub Ahead of print].

Sedlak T, Shufelt C, Iribarren C and Merz CNB (2012) Sex hormones and the QT interval: a review. *J Womens Health* **21**:933-941.

Smith MS, Freeman ME and Neill JD (1975) The control of progesterone secretion during the estrous cycle and early pseudopregnancy in the rat: prolactin, gonadotropin and steroid levels associated with rescue of the corpus luteum of pseudopregnancy. *Endocrinology* **96**:219-226.

Stossi F, Barnett DH, Frasor J, Komm B, Lyttle CR and Katzenellenbogen BS (2004) Transcriptional profiling of estrogen-regulated gene expression via estrogen receptor (ER) α or ERβ in human osteosarcoma cells: distinct and common target genes for these receptors. *Endocrinology* **145**:3473-3486.

Sukumaran S, Jusko WJ, DuBois DC and Almon RR (2011) Mechanistic modeling of the effects of glucocorticoids and circadian rhythms on adipokine expression. *J Pharmacol Exp Ther* **337**:734-746.

Sun YN, DuBois DC, Almon RR and Jusko WJ (1998) Fourth-generation model for corticosteroid pharmacodynamics: a model for methylprednisolone effects on receptor/gene-mediated glucocorticoid receptor down-regulation and tyrosine aminotransferase induction in rat liver. *J Pharmacokinet Biopharm* **26**:289-317.

Sun YN and Jusko WJ (1999) Role of baseline parameters in determining indirect pharmacodynamic responses. *J Pharm Sci* **88**:987-990.

Tsai SY, Tsai MJ and O'Malley BW (1989) Cooperative binding of steroid hormone receptors contributes to transcriptional synergism at target enhancer elements. *Cell* **57**:443-448.

Tynan SH, Lundeen SG and Allan GF (2004) Cell type-specific bidirectional regulation of the glucocorticoid-induced leucine zipper (GILZ) gene by estrogen. *J Steroid Biochem Mol Biol* **91**:225-239.

Whirledge S and Cidlowski JA (2013) Estradiol antagonism of glucocorticoid-induced GILZ expression in human uterine epithelial cells and murine uterus. *Endocrinol* **154**:499-510.

Whirledge S, Xu X and Cidlowski JA (2013) Global gene expression analysis in human uterine epithelial cells defines new targets of glucocorticoid and estradiol antagonism. *Biol Reprod* **89**:66.

Xu ZX, Sun YN, DuBois DC, Almon RR and Jusko WJ (1995) Third-generation model for corticosteroid pharmacodynamics: roles of glucocorticoid receptor mRNA and tyrosine aminotransferase mRNA in rat liver. *J Pharmacokinet Biopharm* **23**:163-181.

Yao Z, DuBois DC, Almon RR and Jusko WJ (2008) Pharmacokinetic/pharmacodynamic modeling of corticosterone suppression and lymphocytopenia by methylprednisolone in rats. *J Pharm Sci* **97**:2820-2832.

Footnotes

This work was supported by the National Institute of General Medical Sciences, National Institutes of Health [Grants GM24211 and GM131800].

FIGURE LEGENDS

Figure 1. Genomic mechanism of corticosteroid regulation of GILZ gene expression in tissues and the influence of estrogens on glucocorticoid signaling. Symbols: hsp 70/90, heat shock protein 70/90; FKBP, FK506 binding protein; GR, glucocorticoid receptor; ER, estrogen receptor; nGRE, negative glucocorticoid response element; RNAP, RNA polymerase.

Figure 2. Schematic of the mPBPK/PD/PG systems model for corticosteroid actions in male and female rats. Parameters and symbols are defined in the text and tables. Lines with arrows indicate blood flows, binding interactions, conversion of species, or turnover of responses. Dashed lines ending in closed boxes indicate inhibition whereas dashed lines with open boxes depict a stimulation of turnover exerted by the connected factors.

Figure 3. Glucocorticoid receptor (GR) mRNA expression at baseline (black bars) and at 4 hours after MPL (gray bars) in livers from 11 wk-old male rats (Cohort 5) and estrus-phased female (Cohort 1) rats (top panel) and in uterus from proestrus (Cohort 2) and estrus (Cohort 1) female rats (bottom panel) determined by qRT-PCR. Error bars reflect one standard deviation from the mean (N = 3 rats/group). *p < 0.05, significant difference between baseline and after dosing at 4 h; *nd*, no significant difference.

Figure 4. Hepatic GR mRNA (left panel) and free cytosolic GR density (right panel) in normal male rats (Cohort 4) after 50 mg/kg IM MPL. The symbols represent the mean ± SD and the solid lines depict the model fit [Eqs. 1-14]. Parameter values are listed in Table 1. Dark (shaded) and light (unshaded) time periods are indicated.

Figure 5. Top panel - plasma 17β-estradiol (E_2) concentrations in non-dosed proestrus and estrus female rats in blood samples taken between 2-6 h after lights ON during each phase and determined using ELISA. Error bars reflect one standard deviation from the mean (N = 4 rats/group). **p < 0.001, significant difference. Middle panel – plasma concentrations of E_2 in female rats over the four-day estrous

cycle; symbols are measurements from individual rats [data taken from Smith et al. (1975)] and the solid line depicts the model-fitted profile [Eq. (18)] shown to repeat for a second cycle. Bottom panel – Simulated profile [Eqs. (20)] of the estrogen complex in the nucleus (ER_N) throughout the rodent estrous cycle in the uterus (left axis) and in liver (right axis). Parameter values are listed in Table 2.

Figure 6. GILZ mRNA expression in liver from male rats (green; top left), estrus-phased female rats (red; top right), and proestrus-phased female rats (blue; top right) given 50 mg/kg IM MPL. Symbols represent the mean ± SD and the solid lines depict the model fit [Eq. (21)]. Parameter values are listed in Table 3. Bottom right – comparison of the model-fitted profiles of hepatic GILZ mRNA in the three groups. Bottom left – comparison of the model-simulated profile of hepatic drug/hormone-receptor complex in the nucleus NR_{N_TOT} [Eq. (6)] in the three groups. Dark (shaded) and light (unshaded) periods are indicated.

Figure 7. GILZ mRNA expression in uterus from estrus-phased female rats (red), and proestrus-phased female rats (blue) given 50 mg/kg IM MPL. Symbols represent the mean ± SD and the solid lines depict the model fit [Eq. (21)]. Parameter values are listed in Table 3. Dark (shaded) and light (unshaded) periods are indicated.

JPET Fast Forward. Published on June 13, 2019 as DOI: 10.1124/jpet.119.257543
This article has not been copyedited and formatted. The final version may differ from this version.

Table 1. Model parameters for glucocorticoid receptor (GR) dynamics.

Parameter	Definition	Estimate (CV%)
$a_{0,GRm,liver}$		14.3
$a_{1,GRm,liver}$		-1.53
$a_{2,GRm,liver}$	Fourier coefficient for liver GR mRNA[a]	0.554
$b_{1,GRm,liver}$		-3.04
$b_{2,GRm,liver}$		1.18
$k_{d,GRm}$ (h^{-1})	Degradation rate constant for GR mRNA	0.14 (17.0)
$IC_{50,GRm}$ (fmol/mg)	Half-maximal inhibition of GR mRNA production	15.2 [a]
τ_{GRm} (h)	Transduction delay for mRNA rebound	15.6 [a]
$IC_{50,TC2}$ (fmol/mg)	Half-maximal inhibition of GR mRNA removal	60.5 [a]
$k_{d,GR}$ (h^{-1})	Degradation rate constant for receptor	0.05 [a]
$k_{on,MPL}$ ($nM^{-1}\cdot h^{-1}$)	Association rate constant for MPL	0.016 [a]
$k_{on,CST}$ ($nM^{-1}\cdot h^{-1}$)	Association rate constant for CST	0.001 (fixed)
$f_{up,mpl}$	Unbound fraction of MPL in plasma	0.4 [b]
$f_{u,liv,mpl}$	Unbound fraction of MPL in liver	0.032 (calculated)
$f_{u,cst}$	Unbound fraction of CST in plasma	0.017 [a]
k_{re} (h^{-1})	DR_N nuclear loss rate constant	1.31 [a]
R_f	Fraction recycled	0.93 [a]
k_T (h^{-1})	Translocation rate constant	58.3 [a]
GR(0) (fmol/mg protein)	Free cytosolic receptor initial concentration	476.0 (liver) [a] 320.0 (uterus) [c]

[a] Fixed from Hazra et al. (2007)

[b] Fixed from Ayyar et al. (2019a)

[c] Fixed from Izawa et al. (1984)

JPET Fast Forward. Published on June 13, 2019 as DOI: 10.1124/jpet.119.257543
This article has not been copyedited and formatted. The final version may differ from this version.

Table 2. Model parameters for plasma 17β-estradiol (E_2) and estrogen receptor (ER) dynamics.

Parameter	Definition	Estimate (%CV) or Value (Source)
Plasma Estradiol Concentrations		
BL (pg/mL)	Baseline concentrations of E_2	6.85 (5.8)
A (pg/mL)	Peak amplitude in met/diestrus	8.6 (14.8)
B (pg/mL)	Peak amplitude in proestrus	32.3 (10.5)
T_{pk1} *(h)*	Time of peak amplitude in met/diestrus	52.3 (3.5)
T_{pk2} *(h)*	Time of peak amplitude in proestrus	82.2 (0.8)
α	Fitting coefficient for first peak	191 (37.5)
β	Fitting coefficient for second peak	106 (16.7)
τ *(h)*	Duration of estrous cycle	96 (fixed)
Estrogen Receptor Binding & Dynamics		
$f_{up,E2}$	Unbound fraction of estradiol in plasma	0.053 (Plowchalk and Teeguarden, 2002)
$B_{max,ER\ (liv)}$ *(fmol/mg protein)*	Estrogen receptor content in liver	24.5 (Aten et al., 1978; Dickson and Eisenfeld, 1979)
$B_{max,ER\ (uterus)}$ *(fmol/mg protein)*	Estrogen receptor content in uterus	560 (Notides, 1970)
$K_{D,ER(liv)}$ *(pM)*	ER Binding Constant in liver	140 (Dickson and Eisenfeld, 1979)
$K_{D,ER(uterus)}$ *(pM)*	ER Binding Constant in uterus	100 (Branham et al., 2002)
k_t *(h^{-1})*	Translocation rate constant	58.3 (Assumed equal to GR)

JPET Fast Forward. Published on June 13, 2019 as DOI: 10.1124/jpet.119.257543
This article has not been copyedited and formatted. The final version may differ from this version.

Table 3. Model parameters for GILZ mRNA dynamics.

Parameter	Definition	Estimate (% CV)
$k_{d,GILZm}$ (h^{-1})	Degradation rate constant for GILZ	7.5 (21.8)[a] ; 1.9 (27.5)[b]
S_{max}	Maximal stimulatory capacity by DR_N	7.5[a,b,c]
$SC_{50,GILZm}$ *(fmol/mg)*	DR_N producing half max stimulation	558 (5.5)[a] ; 672 (19.2)[b]
K_i *(fmol/mg)*	ER_N producing half max inhibition of SC_{50} of DR_N	62.1 (68.6)[a,b]
$GILZ_m(0)$ *(molecules/ng RNA)*	GILZ initial concentration in liver	1893 (M) ; 2051 (E) ; 2538 (PE)
$GILZ_m(0)$ *(molecules/ng RNA)*	GILZ initial concentration in uterus	3245 (E) ; 2400 (PE)

[a] Liver ; [b] Uterus ; [c] Hazra et al. (2008)

JPET Fast Forward. Published on June 13, 2019 as DOI: 10.1124/jpet.119.257543
This article has not been copyedited and formatted. The final version may differ from this version.

Table 4. Area-under-effect-curve (*AUEC*) analysis for GILZ responses.

Group	Baseline (molec/ng RNA)	$AUEC_{obs\ (0\text{-}24h)}$ (molec/ng RNA·h)	$AUEC_{pred\ (0\text{-}24h)}$ (molec/ng RNA·h)
Liver			
Male	1893	31,262	41,952
Female (Estrus)	2051	78,657	73,927
Female (Proestrus)	2538	89,972	93,172
Uterus			
Female (Estrus)	3245	78,828	73,335
Female (Proestrus)	2400	47,340	44,440

JPET Fast Forward. Published on June 13, 2019 as DOI: 10.1124/jpet.119.257543
This article has not been copyedited and formatted. The final version may differ from this version.

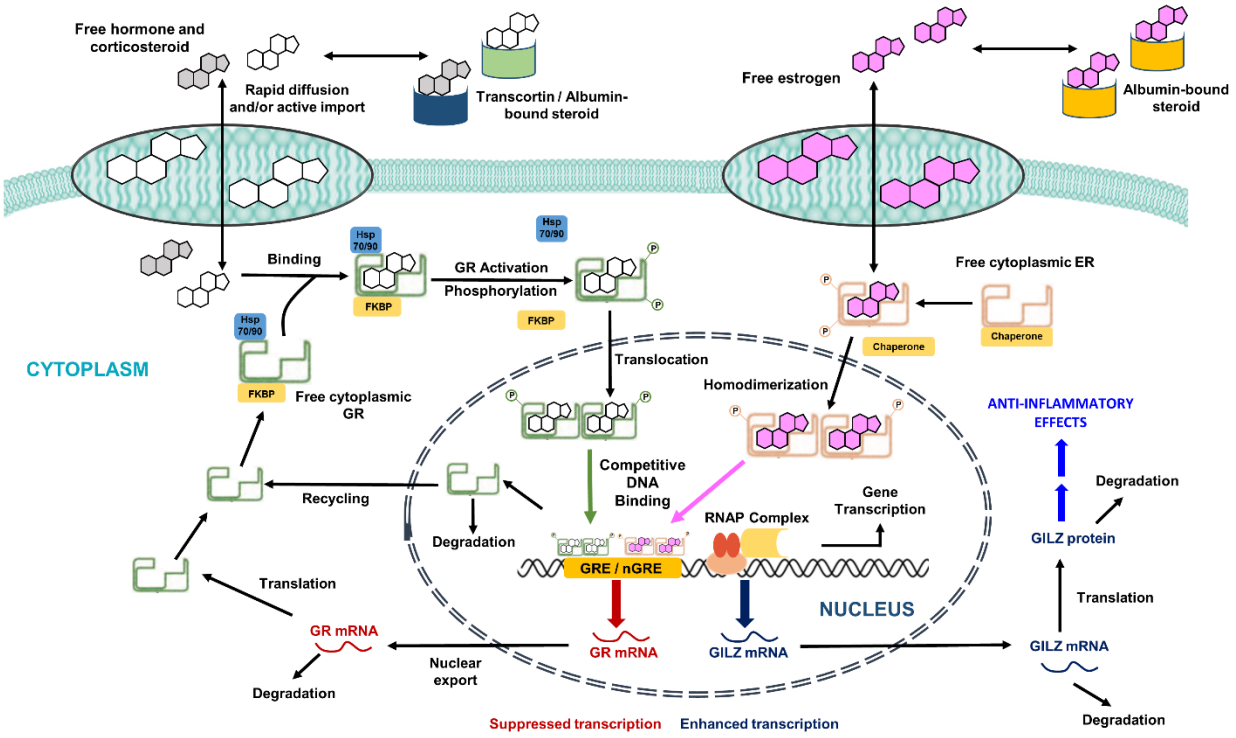

Figure 1

JPET Fast Forward. Published on June 13, 2019 as DOI: 10.1124/jpet.119.257543
This article has not been copyedited and formatted. The final version may differ from this version.

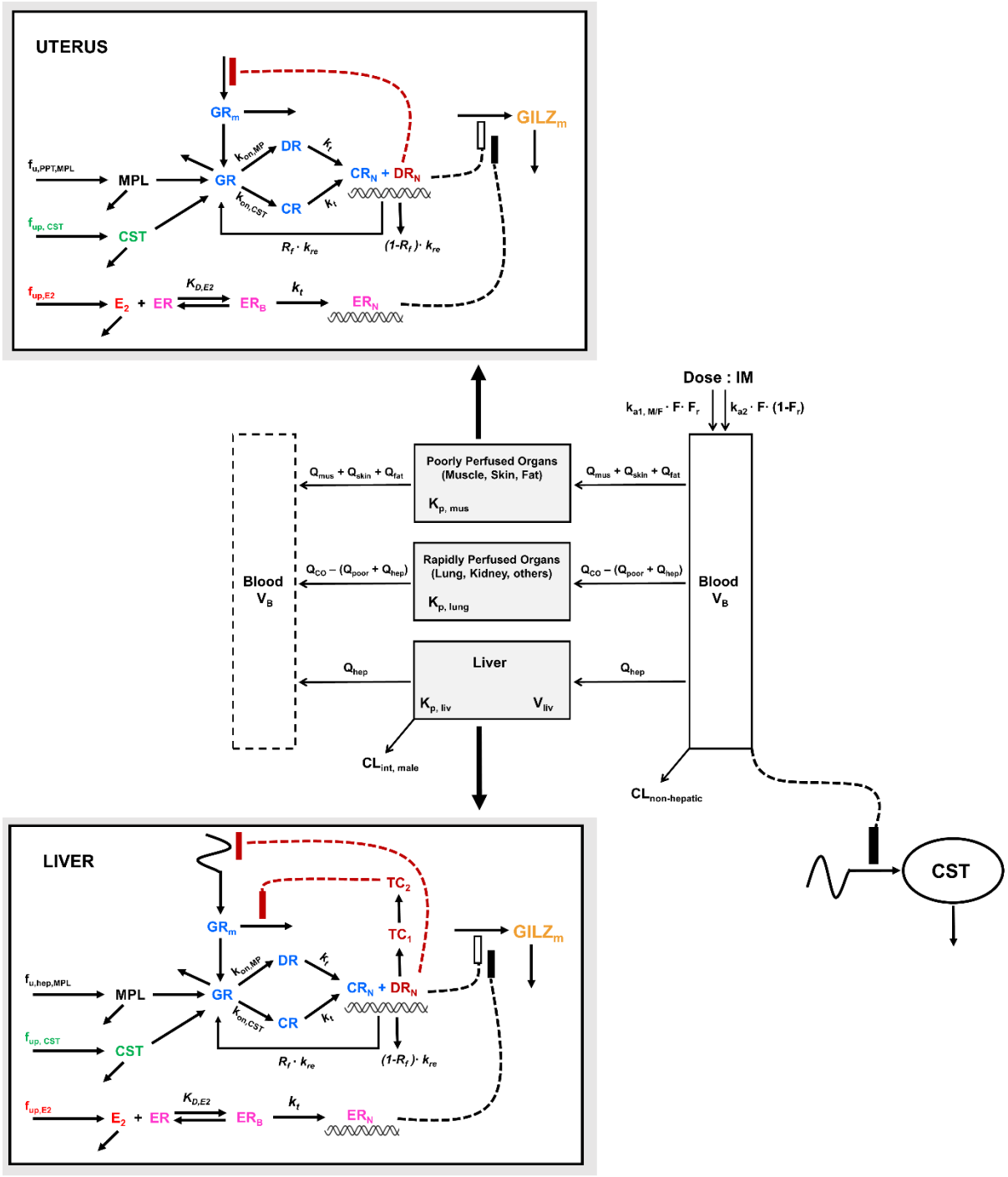

Figure 2

JPET Fast Forward. Published on June 13, 2019 as DOI: 10.1124/jpet.119.257543
This article has not been copyedited and formatted. The final version may differ from this version.

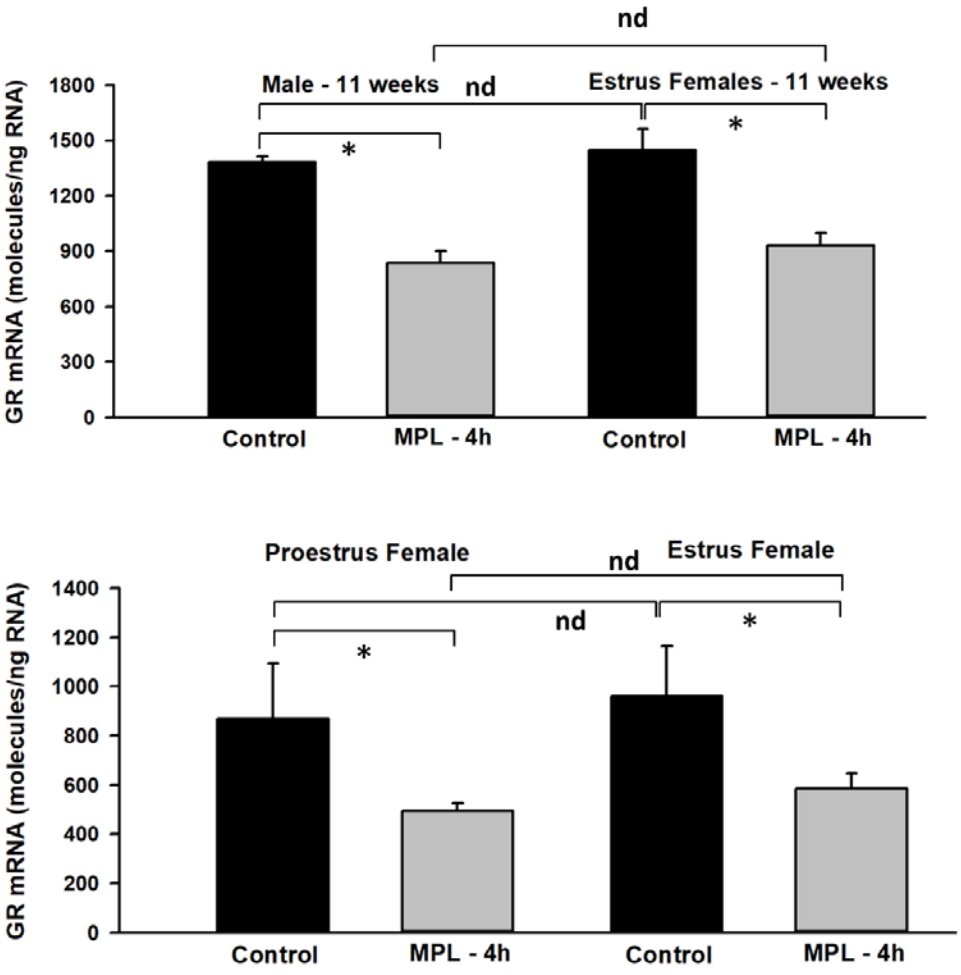

Figure 3

JPET Fast Forward. Published on June 13, 2019 as DOI: 10.1124/jpet.119.257543
This article has not been copyedited and formatted. The final version may differ from this version.

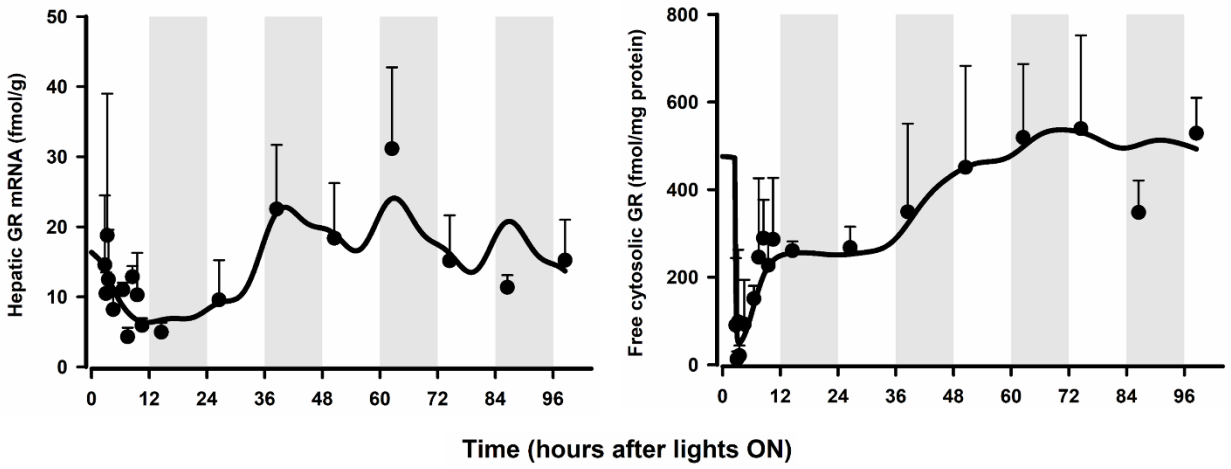

Figure 4

JPET Fast Forward. Published on June 13, 2019 as DOI: 10.1124/jpet.119.257543
This article has not been copyedited and formatted. The final version may differ from this version.

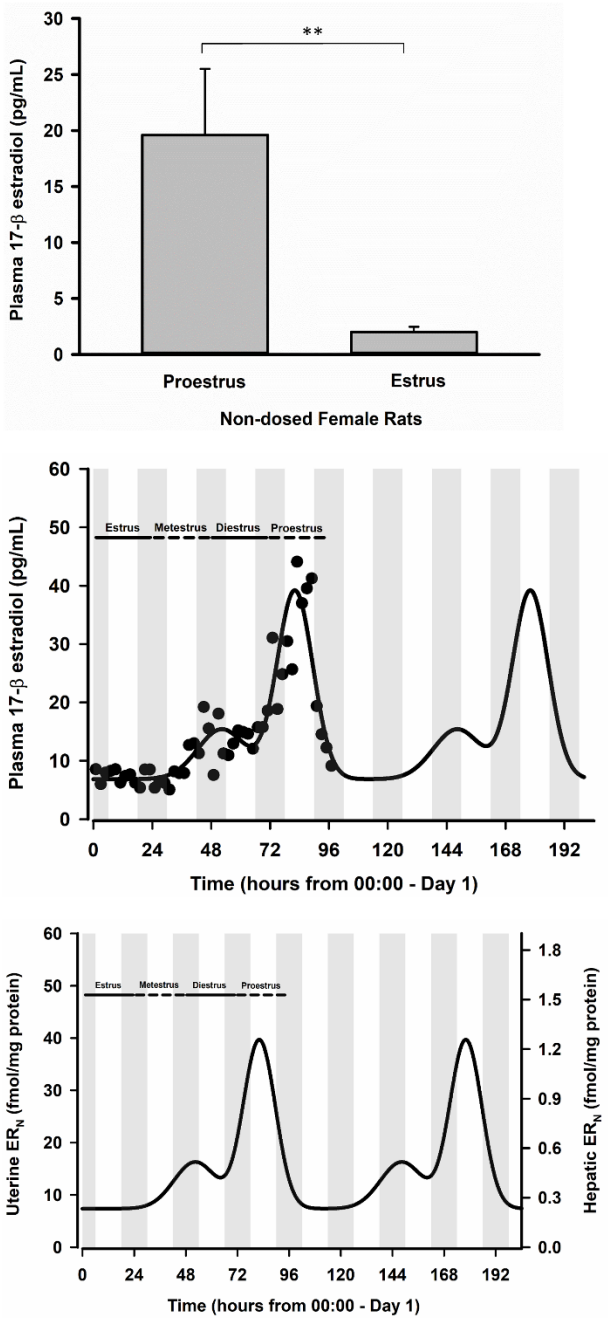

Figure 5

JPET Fast Forward. Published on June 13, 2019 as DOI: 10.1124/jpet.119.257543
This article has not been copyedited and formatted. The final version may differ from this version.

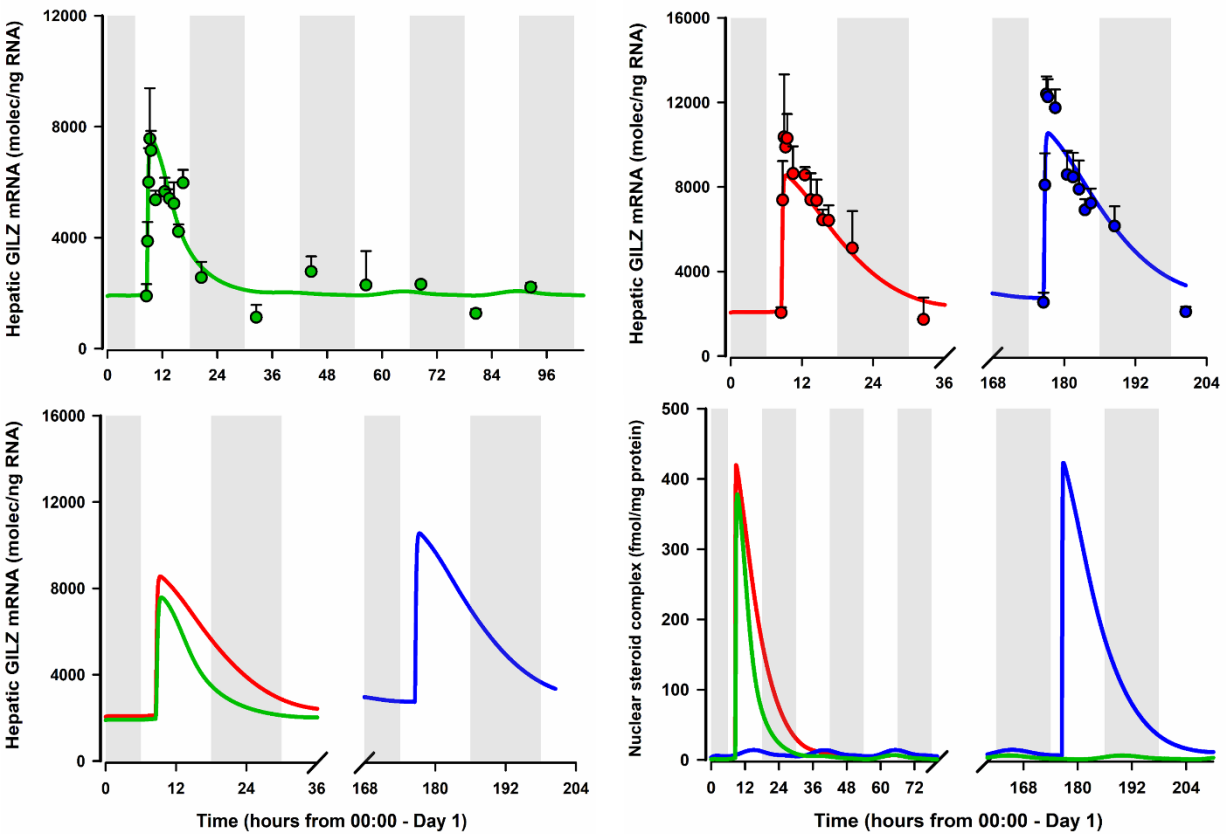

Figure 6

JPET Fast Forward. Published on June 13, 2019 as DOI: 10.1124/jpet.119.257543
This article has not been copyedited and formatted. The final version may differ from this version.

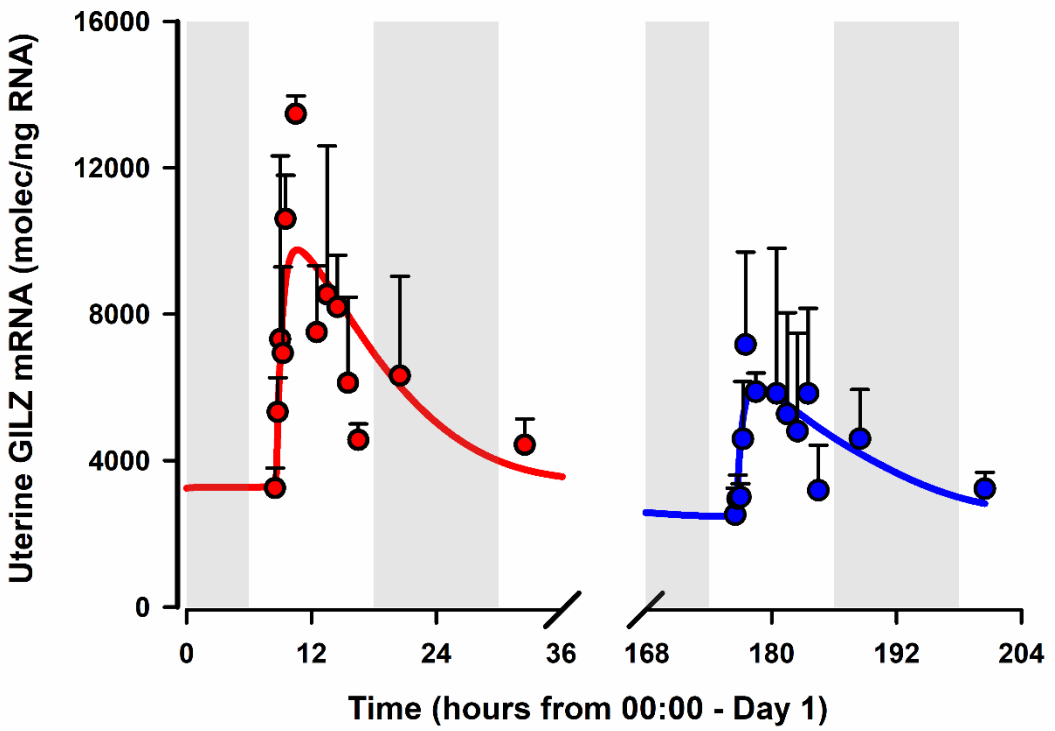

Figure 7